

Optimization of Machining Parameters in Ultra-precision Diamond Turning of Zinc Selenide

Raj Kamal Bharti¹, S.S. Dhami²

^{1,2}Department of Mechanical Engineering, NITTTR, Chandigarh, Chandigarh, India

*e-mail: rajkamal.mech17@nitttrchd.ac.in

Abstract: *Infrared lenses are becoming a vital part of medical and defense applications. Zinc Selenide material is preferable for such applications because of its low absorption of infrared wavelength and high transmissibility of visible light. However, zinc selenide is a brittle material, and therefore polishing and grinding processes are traditionally used to achieve high tolerances in zinc selenide material surface. In this research, a diamond turning machine is used for spherical machining of the Zinc Selenide material. Diamond tool having a negative rake angle and 1.5 mm nose radius are used. The machining parameters have been optimized for achieving a Nano-level surface roughness without grinding and polishing, for optical applications. The effect of the machining parameters on the surface quality of zinc selenide has also been studied.*

Keywords: Zinc selenide, Optimization, Diamond tool, surface roughness

1. Introduction

Brittle materials like zinc selenide, zinc sulfide, glass, ceramics, and germanium are generally used in optical, semiconductor, and other areas. The demand for surface finishing is very rigorous in these applications. The polishing and grinding processes are traditionally used to achieve high tolerances in zinc selenide material surface. **Ying et al. [1]** performed step rough turning, semi-finish turning, and finish turning for optimization of process parameters in aspheric turning of Zinc Sulfide and Zinc Selenide optical lenses. After finish turning, the surface roughness R_a was found less than or equal to 8 nm, the surface shape for ZnS and ZnSe ($\Phi \leq 60\text{mm}$) was found less than or equal to 0.3 μm . The surface shape precision of aspheric Ge ($\Phi \leq 80\text{mm}$) was found less than or equal to 0.3 μm and the surface roughness R_a was found less than or equal to 5 nm. The surface shape precision of Aspheric Si ($\Phi=30\text{mm}$) was found less than or equal to 0.3 μm and surface roughness R_a was found less than or equal to 6 nm. **Fang et al. [2]** investigated the influence of the shape of the cutting edge of the diamond tool on the surface finish of soft semiconductor (ZnS, ZnSe) materials. As the cutting force and thrust force increase, a rougher surface is achieved. The experimental results show that the tool wear mode in the aluminum cutting is different from the tool wear mode in the diamond cutting of zinc selenide. The Nano surface finishes were accomplished, where surface roughness value was $R_a=2.91$ nm on zinc selenide and $R_a=0.88$ nm on Zinc sulfide. **Rhorer & Evans [3]** reported that the diamond turning machine possibly achieves the accuracy of ultraviolet optics fabricated by machining or grinding without post polishing. **Mishra et al. [4]** discussed the effects of several processing parameters, i.e., cutting parameters, tool setting, tool path, and fixture in ultra-precision diamond turning. **V Sarepaka et al. [5]** discussed that the depth of cut, spindle speed and feed rate are the major parameters for obtaining a good surface finish on brittle material. **Ayomoh et al. [6]** investigated that the feed rate is the most dominant effect on the machined surface rather than cutting speed and depth of cut. The ultra-precision single point diamond machining (SPDM) process can produce optics with surface roughness less than tens of nanometers [7-14]. Various researchers have analyzed the behavior of diamond tools in terms of tool wear, but not enough literature is available on tool wear in high precision diamond machining of hard and brittle material such as zinc selenide material [15-22].

1.1 Zinc Selenide

Zinc selenide is one of the most important optoelectronic and electronic material with protuberant applications in flat panels, light-emitting diodes (LED), transistors, nonlinear optical devices, and logic gates, etc [23]. The zinc selenide commonly has two allotropes, hexagonal wurtzite (W) and cubic zinc-blende (ZB) as shown in Fig.1.

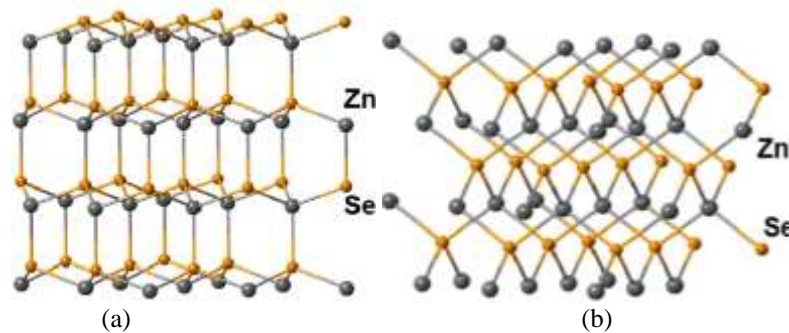


Figure 1: (a) wurtzite crystal structures (W), (b) zinc blende (ZB) [23]

In hexagonal wurtzite (W) the same building blocks are stacked in the ABABAB pattern while ZB consists of tetrahedrally coordinated zinc selenium atoms stacked in the ABCABC pattern. The lattice parameters of hexagonal wurtzite structure are $a=b=3.98 \text{ \AA}$, $c=6.53 \text{ \AA}$ and the lattice parameters of zinc-blende are $a=b=c=5.68 \text{ \AA}$. The difference between the total energy of ZB and W structure is $5.3 \text{ meV atom}^{-1}$. The zinc-blende is the low-temperature ground state structure whereas zinc selenide exhibits the ZB polytypism. The major property of cubic zinc selenide at room temperature as given in Table 1.

Table 1: Material properties of zinc selenide [23]

Molar mass (g/mol)	Density g/cm^3	Melting point ($^{\circ}\text{C}$)	Band gap (eV)	Young Modulus (GPa)	Refractive Index	Optical Dielectric Permittivity
144.35	5.27	1525	2.82 (10K)	67.2	2.67 @550nm	8.7

2. Objective

The objective of the present work is to optimize cutting parameters to achieve a surface roughness of less than 4 nm in ultraprecision diamond turning of Zinc Selenide for optical applications without the subsequent use of any polishing process.

3. Experimental setup

The optical grade flat zinc selenide disk having diameter of 12.7 mm and thickness of 3 mm is used for machining.

In this work, mono-crystalline diamonds with clearance angle 10° and rake angle of -25° are used. The nose radius of 1.5 mm is used to produce fine contour required. The Precitech Nanoform-200 machine was used for single point diamond turning, shown in Fig. 2.

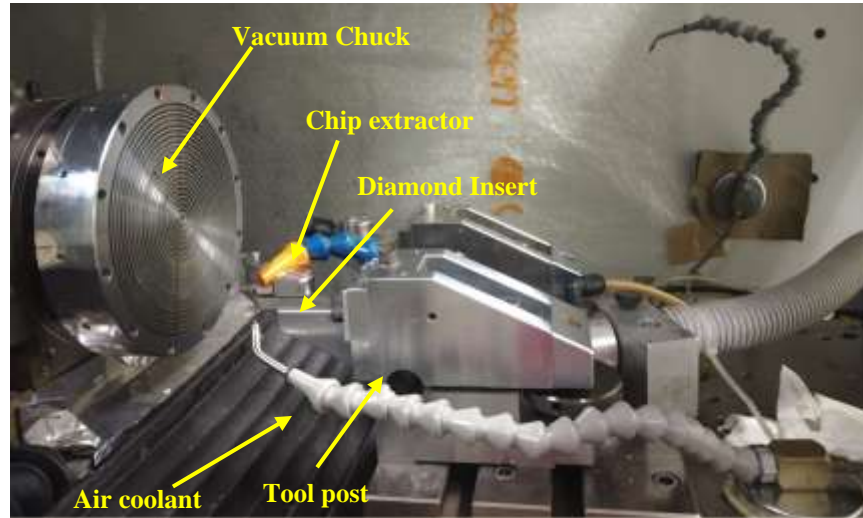


Figure 2: Single Point diamond turning machine

This 3-axis machine is isolated from ambient vibration through a very rigid and stable foundation. Air coolant, vacuum slide environmental sensing system makes the machine versatile and more precise. The device can move 250 mm in the x-axis and 150 mm in the z-axis. The highest working size that the machine can maintain is 250 mm. The work piece is located on vacuum guide ways that can move in the Z-axis during machining application. It is possible to machine flat and spherical surfaces by concurrent command of these three axes.

The Zinc Selenide disc was mounted on the aluminum fixture which was attached to the vacuum chuck. The dial indicator is touched to the fixture's exterior diameter and the portion has been rotated by 360 degrees. Full flood air coolant was used to cool and lubricate the cutting zone to facilitate chips removal from the cutting zone. Parts program was loaded and the Zinc Selenide work-piece was machined.

4. Design of Experiments

The design of experiments was used to generate the required machining combination for evaluation of the contribution of the processing parameters for the efficient performance of the turning process.

Various investigators have used several experimental design techniques for developing regression equations and Central Composite Design (CCD) is reported to be one of the best and precise design techniques. Based on CCD, all the experiments have been conducted, where the lower and upper values were coded as -1 and +1. The face centered CCD contains twenty observations with three input variable i.e. feed rate, depth of cut and spindle speed. In this work, a very fine feed rate (1-5 $\mu\text{m}/\text{min}$), DOC (1-10 μm), and spindle speed (2000-4000 rpm) were used as given in Table 2.

Table 1: Machining processing parameters combination

Parameters	Units	Notation	Range	Levels		
				-1	0	1
Feed rate	$\mu\text{m}/\text{min}$	A	1-5	1	3	5
Depth of cut	μm	B	1-10	1	5.5	10
Spindle speed	rpm	C	2000-4000	2000	3000	4000

5. Results and Discussion

The surface roughness value achieved in the experimentation was measured using CCI Optical Profiler and Non-contact type profilometer followed by developing a mathematical model and optimization of process parameters.

5.1 Experimental Results

The value of surface roughness achieved for different combination of cutting parameter are given in Table 3.

Table 3: Design of experiment and their results

Run	A: Feed rate μm/min	B: depth of cut (μm)	C: Spindle speed (rpm)	Surface roughness (Ra) (nm)
1	3	5.5	3000	9.6
2	1	10	2000	10.2
3	3	5.5	3000	8.1
4	1	1	2000	4.9
5	1	1	4000	5.3
6	1	5.5	3000	12.2
7	5	1	2000	3.2
8	5	10	2000	8.7
9	3	5.5	3000	6.1
10	3	5.5	3000	7.4
11	3	5.5	3000	9.6
12	3	5.5	2000	8.9
13	1	10	4000	10.4
14	5	10	4000	6.7
15	3	5.5	3000	3.9
16	3	10	3000	5
17	3	5.5	4000	8.3
18	5	5.5	3000	7.9
19	3	1	3000	3.8
20	5	1	4000	4.5

From Table 3. The minimum surface roughness (3.2 nm) was observed at feed rate 5 μm/min, depth of cut 1 μm with spindle speed 2000 rpm, whereas maximum surface roughness was obtained at feed rate 1 μm/min, depth of cut 5.5 μm with spindle speed 3000 rpm.

5.2 Developing the mathematical model

Response surface methodology was used to generate a mathematical model. The output response function is surface roughness whereas input parameters are feed rate (A), depth of cut (B), and spindle speed (C). It may be expressed as

$$\text{Surface roughness} = f(A, B, C)$$

The polynomial regression equation of second order which shows the response surface is given by

$$Y = p_0 + \sum p_i x_i + \sum p_{ii} x_i^2 + \sum p_{ij} x_i x_j \quad (1)$$

The selected polynomial can be expressed as

$$Y = p_0 + p_1 A + p_2 B + p_3 C + p_{11} A^2 + p_{22} B^2 + p_{33} C^2 + p_{12} A \times B + p_{13} A \times C + p_{23} B \times C \quad (2)$$

Where P_0 is the average response, coefficient P_1, P_2, P_3 are linear terms, the coefficients P_{11}, P_{22}, P_{33} are quadratic terms, and the coefficient $P_{12}, P_{13},$ and P_{23} are interaction terms. All the coefficients were evaluated and tested for their significance at a 95% confidence level.

The empirical equation developed by ANOVA technique for response variable as shown in eq.2. The actual experimental surface roughness process parameters and their levels are shown in table 3. The developed model was evaluated by Fisher's F-test at a 95% confidence level using design expert software. As per model adequacy, the standard Fisher's (F) value must be more than the calculated value of F. Models are significant when the lack of fit is not significant. The ANOVA's for the responses for surface roughness were reported in tables 4. The surface roughness (R_a) is represented as a function of feed rate (A), depth of cut (B), and spindle speed (C). The developed final mathematical empirical equation in the coded form has been given below

$$\text{Surface roughness} = 9.45 - 3.28A + 2.77B - 0.003 C - 0.0375 AB + 0.52 A^2 - 0.176 B^2 \quad (3)$$

Table 4: ANOVA for surface roughness (surface quadratic model)

Source	Sum of Squares	df	Mean Square	F-value	p-value	
Model	91.39	9	10.15	3.08	0.00172	Significant
A-Feed rate	14.4	1	14.4	4.37	0.0632	
B-depth of cut	37.25	1	37.25	11.3	0.0072	
C-Spindle speed	0.049	1	0.049	0.0149	0.9054	
AB	0.9112	1	0.9112	0.2763	0.6106	
AC	0.2113	1	0.2113	0.0641	0.8053	
BC	1.53	1	1.53	0.4643	0.5111	
A ²	11.97	1	11.97	3.63	0.0859	
B ²	34.92	1	34.92	10.59	0.0087	
C ²	1.11	1	1.11	0.3377	0.574	
Residual	32.98	10	3.3			
Lack of Fit	8.88	5	1.78	0.3686	0.8513	not significant
Pure Error	24.09	5	4.82			
Cor Total	124.37	19				
Std. Dev.	1.82	R ²	0.7348			
Mean	7.23	Adjusted R ²	0.4962			
C.V. %	25.10	Predicted R ²	0.0707			
		Adeq Precision	6.8375			

The ANOVA table for surface roughness with respect to selective variables reveals that Fisher's (F) value is 3.08 which shows that the model is significant. The chance of F value due to error is only 0.17% as per the p-value. In the mathematical model, the product of p-value of feed rate (A) and depth of cut (B) is less than 0.6106 which shows these terms to be significant. The coefficient of R² shows the goodness of fit of the model. The R² (0.7348) value for surface roughness shows that 73.48% of the complete variability is analyzed by the model after considering the significant factor. The difference between R² (73.48%) and adjusted R² (49.62%) is 23.86%, which shows that 23.86% of the total variation is not elucidated by the model and it also indicates that the model is not over fitted. 3D response surface plot and contour of surface roughness are shown in Fig. 3.

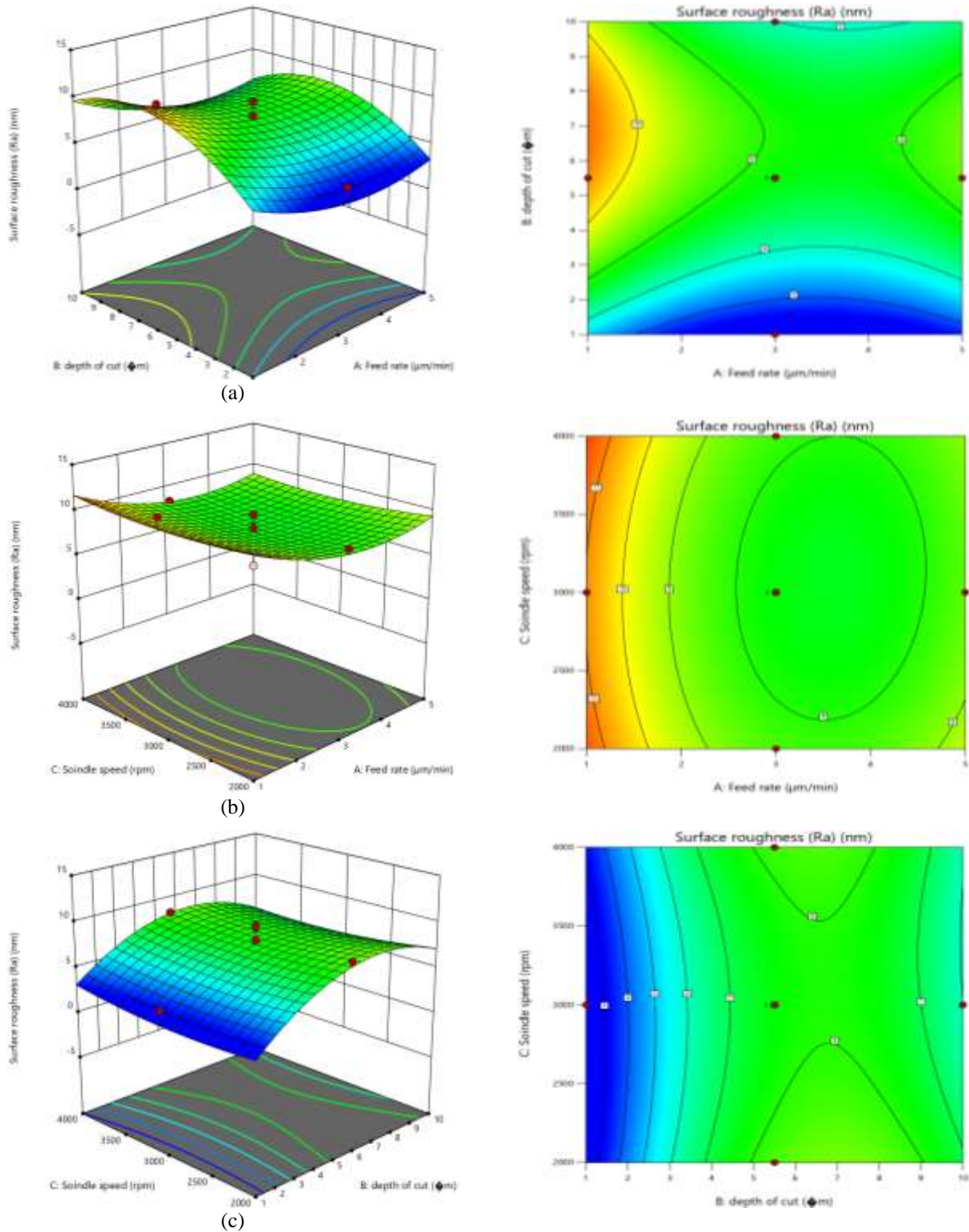


Figure 3: 3D response surface plot and contour plot for surface roughness

When the feed rate increases and depth of cut decreases, the surface roughness decreases due to strain hardening effect caused by tool stirring. When feed rate increases and spindle speed decreases, then the surface roughness decreases. As the depth of cut increases, and spindle speed decreases, then the surface roughness first increases then decreases. The predicted vs. experimental values for surface roughness is shown in Fig. 4

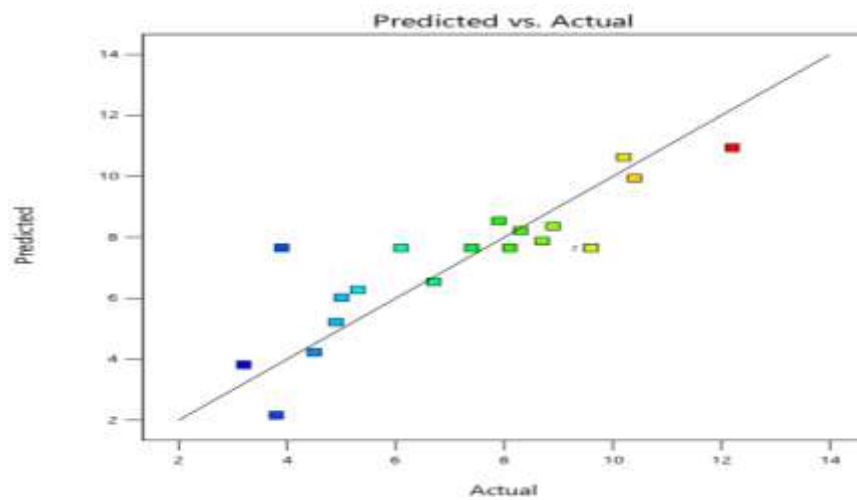


Figure 4: Predicted vs. experimental value for surface roughness

The response variable is lying on the straight line which indicates that the error is uniformly scattered throughout the model. This plot shows an excellent correlation between predicted and experimental values of the response values. All the above correlation divulges the good adequacy of the regression models. The ramp function of multi-response optimization as shown in Fig. 5.

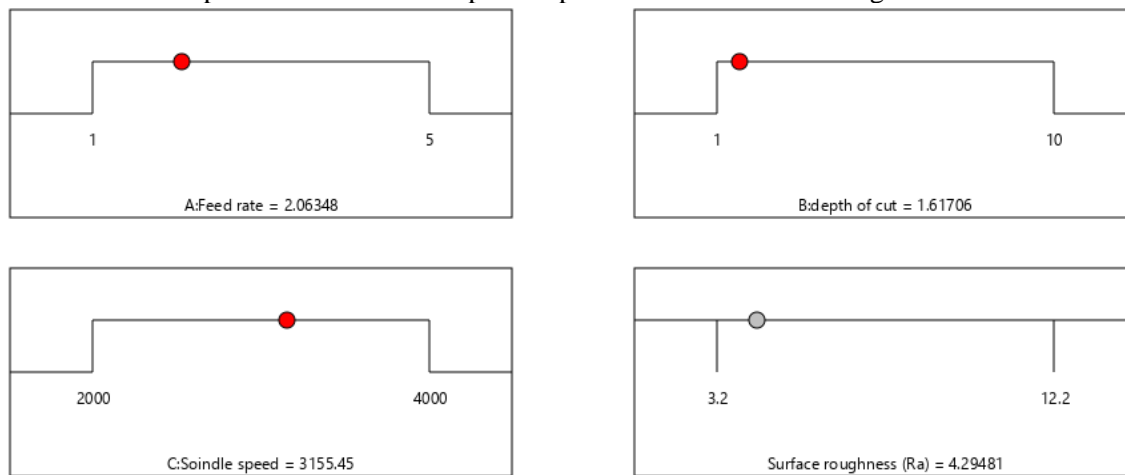


Figure 5: Ramp function graph for input parameter and Multi response optimization

The design expert software computes the point prediction optimal range at 95% tolerance interval (TI) and 95% confidence interval for different responses as given in Table 5.

Table 5: Point prediction at optimal responses

Predicted Mean	Predicted Median	Std Dev	SE Mean	95% CI low for Mean	95% CI high for Mean	95% TI low for 99% Pop	95% TI high for 99% Pop
4.2948 1	4.2948 1	1.8159 7	1.0254 8	2.01	6.57972	-5.01566	13.6053

This methodology is used to optimize for more than one objective function. The desirable value is 1 for the optimized value of the input processing parameters and responses. The optimized value of surface roughness is 4.294 nm, whereas the optimized value of feed rate, depth of cut, and spindle speed are 2.06 $\mu\text{m}/\text{min}$, 1.617 μm and 3155.45 rpm as per the ramp function. However, a lower surface roughness of 3.2 nm was obtained experimentally for experiment number 7, corresponding to which feed

rate of 5 $\mu\text{m}/\text{minute}$, depth of cut of 1 μm and spindle speed of 2000 RPM were selected as optimum cutting parameters.

Fig.6 and fig.7 show the surface roughness and surface morphology of the zinc selenide disc at the best and worst combination of machining parameters respectively.

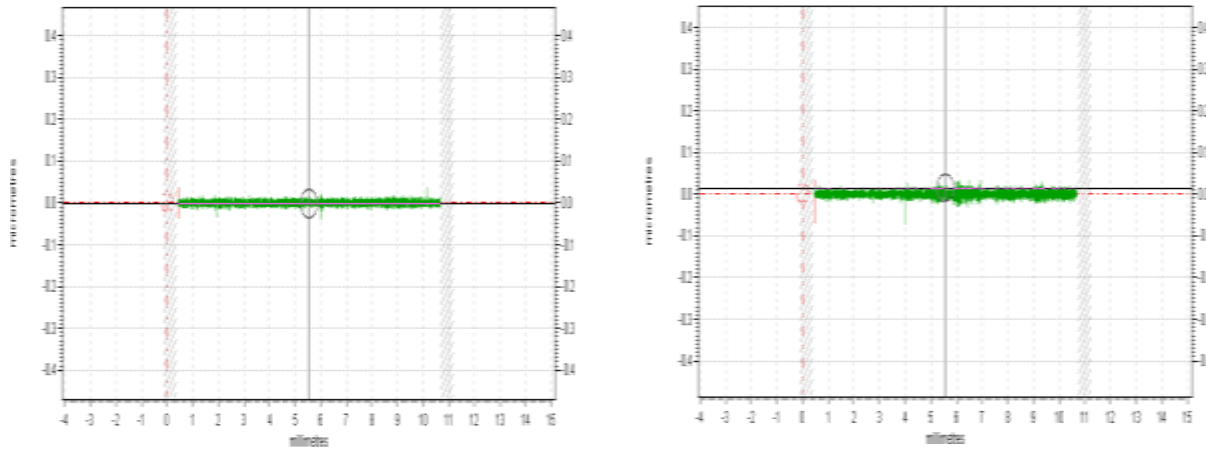


Figure 6: Surface roughness profile, (a) experiment No.7, (b) experiment No.6

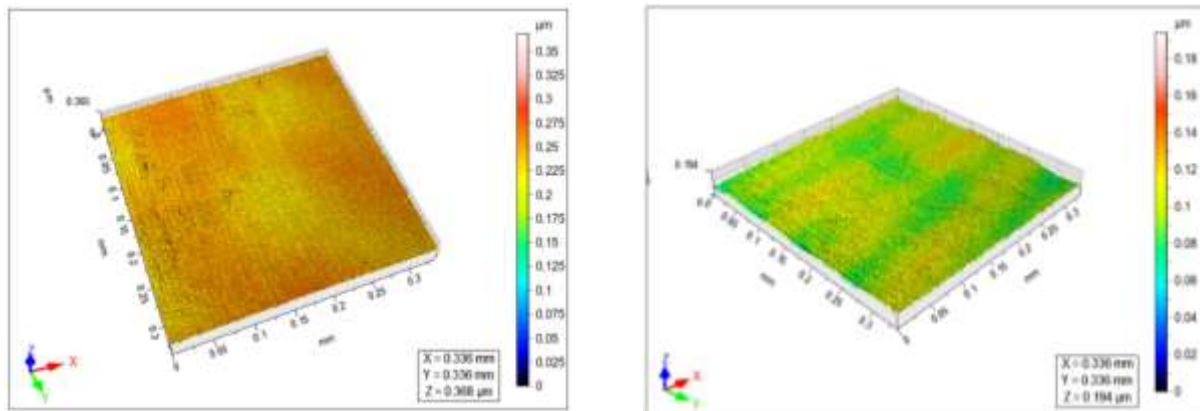


Figure7: Surface morphology, (a) best combination, (b) worst combination

The minimum and maximum surface roughness (3.2 nm) achieved at different combinations are 3.2 nm and 12.2 nm respectively. The effect of spindle speed and DOC on surface roughness experiments 6 and 13 with the same feed rate but different depth of cut shows the surface roughness of 12.2 nm and 10.4 nm respectively, whereas minimum surface roughness (3.2 nm) was obtained at feed rate 5 $\mu\text{m}/\text{min}$, DOC 1 μm , and spindle speed 2000 rpm.

Fig.8 shows the FESEM images of zinc selenide chips collected in the first facing cuts for the negative rake angle tools.

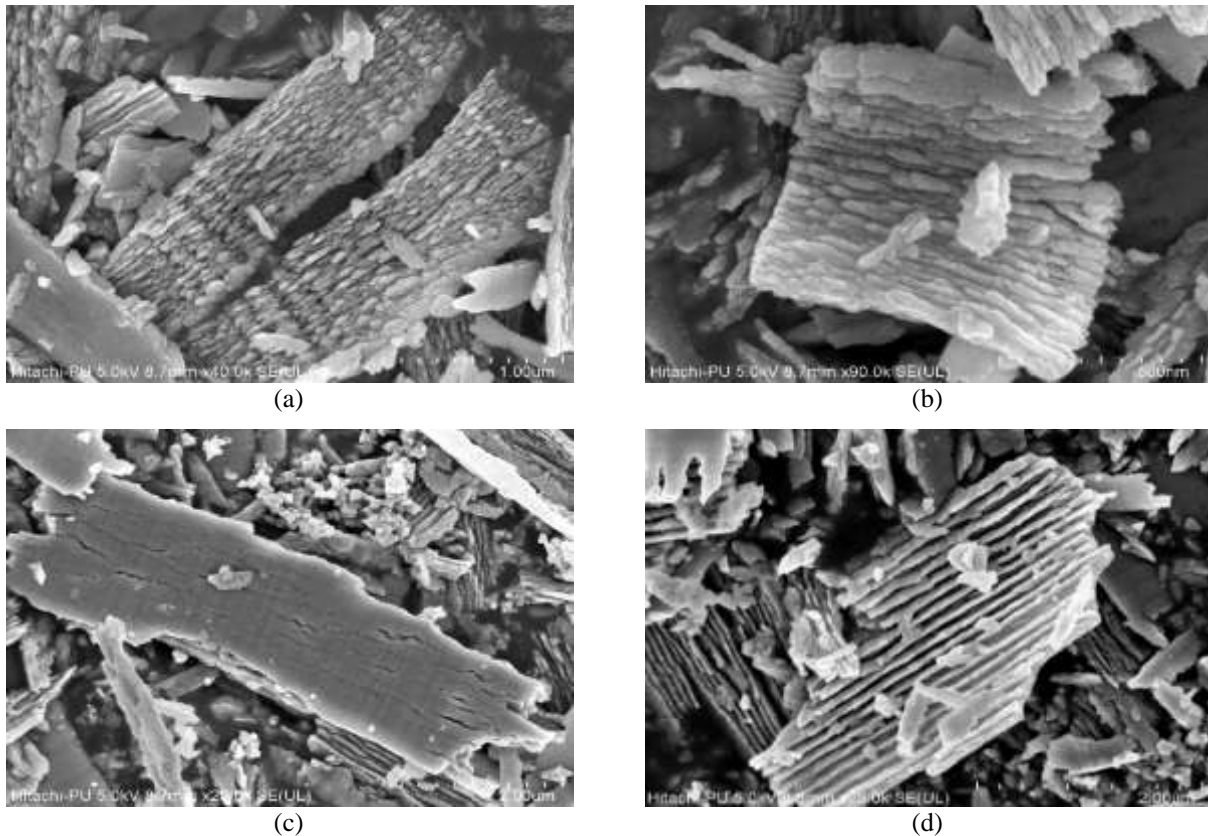


Figure 8: FESEM Nano graphs of chip for experiment 6, (a), (b) and experiment 7 (c), (d)

FESEM nanograph of experiments 6, (a) (b) and experiment 7, (c) (d) clearly shows that the chip formation was observed in experimental studies of zinc selenide. For -25° rake angle tool, chips were mainly formed in combination with continuous and broken chips along with the dominant powder form. Smoother and longer ribbon type chips were observed using -25° rake angle tool. The distortion could possibly be due to the flow of chip under the tool with high compressive stresses.

6. Conclusions

In the present work a very low surface roughness of 3.2 nm is achieved in turning of Zinc Selenide Optical material using Diamond cutting tool and optimizing the cutting parameters using Response Surface Methodology (RSM) approach. The optimum cutting parameters corresponding to minimum surface roughness are feed rate of 5 $\mu\text{m}/\text{minute}$, depth of cut of 1 μm and spindle speed of 2000 RPM. The cutting tool had a rake angle of -25° and corner radius of 1.5 mm. The experimental work and analysis of the results reveals that the DOC and feed rate were the most dominant factor in surface roughness for zinc selenide. Smooth and long ribbon type chips were observed using -25° rake angle tool.

References

- [1] Su Ying, Chen Xianhe, Guo Xiaogang, Guo Rui, Liu Xuanmin, Zhang feng, Yang Chao, Xiao Yingyu, Xu Zengqi, "New Fabrication technology in single point diamond turning for IR aspheric optical parts" 7th International Symposium on Advanced Optical Manufacturing and Testing Technologies, 2008 ,SPIE Vol. 9281, 92811L.
- [2] F. Z. Fang, V. C. Venkatesh and G. X. Zhang, "Diamond Turning of Soft Semiconductors to Obtain Nanometric Mirror Surfaces" *The International Journal of Advanced Manufacturing Technology*, 2000, Volume 19, Issue 9, pp 637–641.
- [3] Richard L. Rhorer and Chris J. Evans, "Fabrication of optics by diamond turning" *Handbook of optics*, 1995.

- [4] Vinod Mishra, Harry Garg, Vinod Karar and Gufran S. Khan, "Ultra-precision Diamond Turning Process" *Micro and Nano Machining of Engineering Materials*, **2018**, pp 65-97.
- [5] RamaGopal V Sarepaka, Rajesh Singh Panwar, Siva Sakthibalan, SomaiahDudala, RajendraKotaria, "Brittle Machining Issues in Single Point Diamond Turning of Aspheric Infra-Red Optics" *10th international conference on precision mesho, micro and nano engineering (COPEN10)*,**2015**.
- [6] M. Ayomoh, K Abou. El Hussein, "Surface finish in ultra precision diamond turning of single crystal silicon." *Proc SPIE*, **2015**, Vol. 9633.
- [7] Furukawa, Y., and Moronuki, N., **1988**, "Effect of Material Properties on Ultra Precise Cutting Processes," *CIRP Ann.*, 37, pp. 113–116.
- [8] Yuan, Z. J., Lee, W. B., Yao, Y. X., and Zhou, M., **1994**, "Effect of Crystallographic Orientation on Cutting Forces and Surface Quality in Diamond Cutting of Single Crystal," *CIRP Ann.*, 43, pp. 39–42.
- [9] Revel, P., Khanfir, H., and Fillit, R. Y., **2006**, "Surface Characterization of Aluminum Alloys After Diamond Turning," *J. Mater. Process. Technol.*, 178, pp. 154–161.
- [10] Hocheng, H., and Hsieh, M. L., **2004**, "Signal Analysis of Surface Roughness in Diamond Turning of Lens Molds," *Int. J. Mach. Tools Manuf.*, 44, pp. 1607–1618.
- [11] Kim, J. D., and Kim, D. S., **1996**, "Surface Characteristics of Magnetic-Disk Cutting Using a Single-Crystal Diamond Tool in an Ultraprecision Lathe," *J Mater. Process. Technol.*, 59, pp. 303–308.
- [12] Ogloza, A. A., Decker, D. L., Archibald, P. C., O'Connor, D. A., and Bueltmann, E. R., **1988**, "Optical Properties and Thermal Stability of Single-Point Diamond Machined Aluminum Alloys," *Proc. SPIE*, 966, pp. 228–251.
- [13] Cheung, C. F., and Lee, W. B., **2003**, *Surface Generation in Ultra-Precision Diamond Turning: Modelling and Practices*, Professional Engineering Publishing, Wiltshire, UK.
- [14] Roblee, J. "Factors Affecting Surface Finish in Diamond Turning", www.precitech.com/Factorsaffectingsurfacefinish.pdf.
- [15] Ohta T, Yan J, Sunao Kodera , Yajima Shuuma, Horikawa Naoyuki, Takahashi Youichi, Kuriyagawa T (2009) Coolant effects on tool wear in machining single-crystal silicon with diamond tools, in *Key Eng Mater: 144–150*, 505
- [16] Uddin MS, Seah KHW, Rahman M, Li XP, Liu K (2007) Performance of single crystal diamond tools in ductile mode cutting of silicon. *J Mater Process Technol* 185(1):24–30
- [17] Zhou M, Ngoi BKA, Yusoff MN, Wang X (2006) Tool wear and surface finish in diamond cutting of optical glass. *J Mater Process Technol* 174(1–3):29–33
- [18] Yoshino M, Nakajima S, Terano M (2015) Tool wear of a single-crystal diamond tool in nano-groove machining of a quartz glass plate. *Surf Topogr: Metrol Prop* 3(4):1–11
- [19] Saurav G, Xichun L, Robert LR, Pen H (2012) Influence of temperature and crystal orientation on tool wear during single point diamond turning of silicon. *Wear* 284:28565–28572.
- [20] Dumas D, Fendler M, Berger F, Cloix B, Pornin C, Baier N et al (2012) Infrared camera based on a curved retina. *Opt Lett* 37(4): 653–655.
- [21] Fang Z and Zhao CZ (2012) Recent progress in silicon photonics: a review. *ISRN Optics*
- [22] Suleski TJ, Davies MA and Dutterer BS (2012) Diamond machining of freeform infrared optics. in *Optical Fabrication and Testing: OW2D*.
- [23] Qi Zhang, Huiqiao Li, Ying Ma, Tianyou Zhai, ZnSe nanostructures: Synthesis, properties and applications, *Progress in Materials Science* 83 (2016) 472–535.
- [24] C.F. Cheung, W.B. Lee, A theoretical and experimental investigation of surface roughness formation in ultra-precision diamond turning, *International Journal of Machine Tools & Manufacture* 40 (2000) 979–1002.
- [25] D.J. Whitehouse, *Handbook of Surface Metrology*, Bristol, Philadelphia: Institute of Physics Pub., **1994**.
- [26] T. Sata, M. Li, S. Takata, H. Hiraoka, C.Q. Li, X.Z. Xing, X.G. Xiao, Analysis of surface roughness generation in turning operation and its applications, *Annals of the CIRP* 34 (1985) 473–476.